Experimental Demonstration of Peak Wavelength Measurement of Multiplexing Fiber Bragg Gratings Using Convolutional Neural Network

Tatsuya Yamaguchi, *Member, IEEE*, Hiroto Kawashima, Hiroki Matsuda, and Yukitaka Shinoda, *Member, IEEE*

***Abstract*—We propose a peak detection method for measuring fiber Bragg gratings (FBGs) using convolutional neural network (CNN) to improve the performances of wavelength division multiplexing. In wavelength division multiplexing, each FBG occupies a certain wavelength range; therefore, the number of FBGs that can be installed is limited by the wavelength band of the light source. To address this issue, methods for overlapping multiple FBGs of the same wavelength within a single occupied wavelength range have been studied. This contributes to improving the limit of multipoint FBG's manifold. However, this method results in the complex overlapping of multiple FBG reflectance spectra, making it difficult to accurately measure the peak wavelengths of individual FBGs using conventional peak detection methods. Therefore, we developed a peak detection process using CNN, which is suitable for identifying unique feature data. Each FBG of the same wavelength was characterized to have a unique spectral shape by assigning a different full-width at half-maximum (FWHM) values to each. We introduced noise-additive learning, a well-known method of data augmentation that increases tolerance to variations in the experimental signal. As a result, the standard deviation for peak wavelength detection significantly improved to 2.8 pm and the strain measurements with three complex overlapping FBGs were successfully demonstrated. The CNN model is the first to solve the problem of three overlapping FBGs for arbitrary wavelength changes. Furthermore, the developed peak detection process was found to be applicable to measurements that combined multiplexing of FBGs of either identical or different wavelengths.**

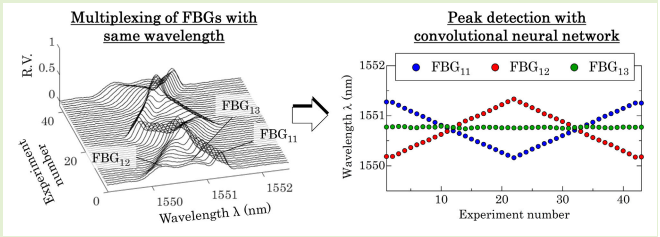

***Index Terms*— Convolutional neural networks (CNNs), deep learning, fiber Bragg gratings (FBGs), optical fiber sensors, wavelength division multiplexing.**

I. Introduction

OPTICAL fiber sensors have excellent performance. They are explosion-proof and corrosion-resistant, and have been attracting attention owing to the demand for monitoring social infrastructure [1], [2], [3], [4], [5], [6]. Among them, fiber Bragg gratings (FBGs) are capable of multipoint measurement of strain and temperature using inexpensive and simple optical devices and are applied in a wide range of fields, such as aerospace, defense, and energy. FBG is an optical fiber sensor that reflects light of Bragg wavelength, and its wavelength varies in proportion to strain and temperature [7], [8], [9], [10], [11], [12].

A typical method of multiplexing FBGs is to use wavelength-division multiplexing and assigning occupied wavelength ranges to individual FBGs [7], [13], [14]. However, there is a limit to the number of occupied wavelength regions that can be allocated within the wavelength band of a typical light source, making the multiplexing of increasing multipoint FBGs challenging. Under these circumstances, a method for installing multiple FBGs of the same wavelength within one occupied wavelength range has been proposed. This is expected to improve the multipoint limit several times over. In this method, multiple FBG reflectance spectra with a complex overlap were observed. Therefore, it is difficult to

Manuscript received 16 February 2023; accepted 11 March 2023. Date of publication 3 April 2023; date of current version 1 May 2023. This work was supported in part by the Japan Society for the Promotion of Science (JSPS) KAKENHI under Grant 20K14754 and in part by the Nihon University College of Science and Technology for Research. The associate editor coordinating the review of this article and approving it for publication was Prof. Agostino Iadicicco. *(Corresponding author: Tatsuya Yamaguchi.)*

Tatsuya Yamaguchi and Yukitaka Shinoda are with the Department of Electrical Engineering, College of Science and Technology, Nihon University, Tokyo 1010062, Japan (e-mail: yamaguchi.tatsuya@nihon-u.ac.jp; shinoda.yukitaka@nihon-u.ac.jp).

Hiroto Kawashima and Hiroki Matsuda are with the Department of Electrical Engineering, Graduate School of Science and Technology, Nihon University, Tokyo 1010062, Japan (e-mail: cshi22013@g.nihon-u.ac.jp; cshi22035@g.nihon-u.ac.jp).

Digital Object Identifier 10.1109/JSEN.2023.3262494

accurately measure the peak wavelength of individual FBGs using conventional peak detection methods such as maximum value and center-of-gravity detection. Several methods have been considered and discussed to solve this problem.

One proposed solution is to use a frequency-modulated continuous-wave radar (FMCW) [15], [16]. This method uses interferometric optics and analysis in the frequency domain to separate overlapping FBGs. Therefore, the analysis can be performed using conventional peak detection. However, there are issues that impose restrictions on their measurement, such as the need to configure interference optics. This makes the equipment complex and expensive and the sensor more sensitive to ambient disturbances [17]. Further research is underway to address these issues. In contrast, studies have reported peak detection methods that directly analyze the reflectance spectra of overlapped FBGs without special optical adjustments, such as interference optics in the equipment [18], [19], [20], [21], [22], [23], [24]. These methods only require the incorporation of peak detection processing in the optical system and are expected to significantly improve the multipoint performance at a low cost.

Artificial intelligence (AI) has made remarkable progress in recent years, achieving performance rivaling that of humans in areas such as image and voice recognition. The spread of the technology continues unabated, and even in the field of optical fiber sensors, research has been reported to achieve measurement performance superior to conventional methods by introducing AI technology [25], [26], [27]. Under these circumstances, it is clear that AI could provide a breakthrough in the development of peak detection methods. AI is useful in identifying unique features. Therefore, for each overlapped FBG, parameters such as reflectance and full-width at half-maximum (FWHM) were adjusted to provide a unique reflectance spectral shape. This enabled highly accurate peak detection of individual FBGs at the same wavelength. Genetic algorithms, decision trees, and support vector regression have been proposed as methods for peak detection [18], [19], [20], [21]. Among them, deep learning, with its high learning capability, has been reported to enable picometer resolution and millisecond computation time. Additionally, it has the potential for unprecedented high-performance multipoint sensing [22], [23], [24]. Recent studies using AI have reported a variety of important findings. However, current research has been verified under the constraints of fixed wavelength of one of the two overlapping FBGs or changing wavelength in a unidirectional and linear manner in the direction of the longer wavelength. Therefore, measurement with a high degree of freedom to accommodate arbitrary wavelength changes in which individual FBGs operate independently, which is required in actual measurements, has not been reported. To realize such measurements, it is necessary to consider the problem of varying the independent wavelengths of individual FBGs, and a new peak detection method that can handle more complex overlaps must be proposed. In addition, the working of more than two overlapping FBGs should be experimentally demonstrated to observe the improvement in the multipoint performance.

This study uses a convolutional neural network (CNN), a type of deep learning algorithm, to demonstrate multi-

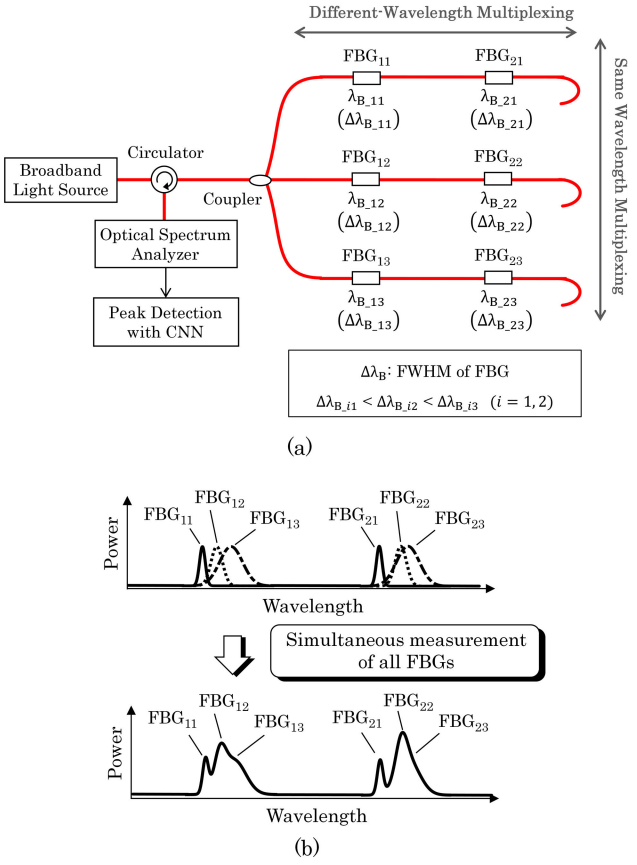

Fig. 1. FBG measurement system with CNN. (a) Measurement system. (b) Spectrum of multiplexed FBGs.

point measurements with three overlapping FBGs. CNN is a powerful method for extracting unique features using convolutional filters, and its high accuracy has been reported in medical imaging and signal data analysis [28], [29]. Therefore, in this experiment, peak detection of individual FBGs was made possible by assigning a unique FWHM to each FBG to provide unique characteristics. The training data for the CNN were generated by creating a numerical model of the FBG using the Gaussian approximation. The validation results of the FBG multipoint measurements revealed a large difference in the standard deviations for peak wavelength detection of the numerical simulations and experiments. To increase the tolerance to variations in the experimental signal, we introduced noise-additive learning, which is a well-known method of data augmentation in the field of image processing [30], [31]. This significantly improves the standard deviation for peak wavelength detection by 2.8 pm. Consequently, strain measurements with three FBGs multiplexed at the same wavelength were successfully performed. Furthermore, multiple and simultaneous FBG measurements were achieved in the 1550 and 1555 nm wavelength regions, demonstrating the feasibility of combining same-wavelength and different-wavelength multiplexing.

II. Experimental Setup

A. Measurement System With CNN

Fig. 1(a) shows the FBG measurement system with a CNN. The optics setup has a very simple configuration. The

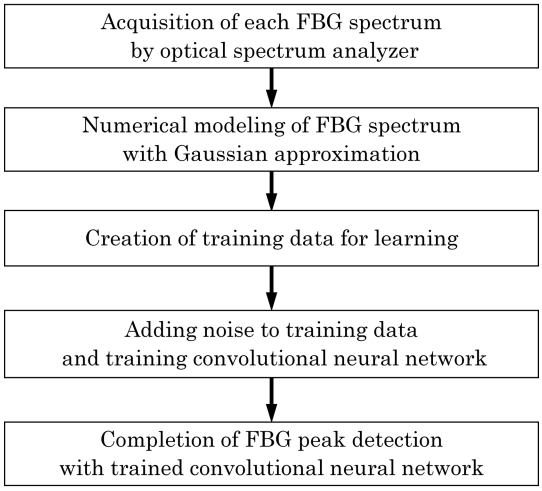

Fig. 2. Design flow of peak detection with CNN.

broadband light source (Lightwaves 2020) is a fiber-optic type doped with erbium ions and has a central wavelength of approximately 1550 nm. The light from the broadband light source was split by the coupler through the circulator and entered the FBG sensor. Six FBGs were used in the experiment. FBG_{11}, FBG_{12}, and FBG_{13} have Bragg wavelengths λ_{B_11}, λ_{B_12}, and λ_{B_13} of 1550 nm, reflectance of approximately 3%, and FWHM $\Delta\lambda_{B\_11}$, $\Delta\lambda_{B\_12}$, and $\Delta\lambda_{B\_13}$ of approximately 0.2, 0.4, and 0.7 nm, respectively. FBG_{21}, FBG_{22}, and FBG_{23} have Bragg wavelengths λ_{B_21}, λ_{B_22}, and λ_{B_23} of 1555 nm, reflectance of approximately 3%, and FWHM $\Delta\lambda_{B\_21}$, $\Delta\lambda_{B\_22}$, and $\Delta\lambda_{B\_23}$ of approximately 0.2, 0.4, and 0.7 nm, respectively. In this experiment, the Bragg wavelength of the FBG was selected for the central wavelength region of the light source. The Bragg wavelengths of 1550 and 1555 nm were selected to ensure a sufficient wavelength margin to void interference between the FBGs. The FBGs of the same wavelength were characterized by assigning a unique FWHM. The reflected light from each FBG entered the optical spectrum analyzer through the circulator. The optical spectrum analyzer (AQ6317B, Ando) acquires FBG spectra in the wavelength range of 1549.2–1557.5 nm with an output resolution of 2 pm. The acquired spectra were smoothed by applying a Gaussian filter as a pre-processing step. Each FBG had a unique FWHM, as shown in Fig. 1(a). Therefore, as shown in Fig. 1(b), three FBGs with different FWHMs were observed in a complex overlapping spectrum. The FBGs at different wavelengths were observed separately in the 1550 and 1555 nm wavelength regions. The observed results were used in the peak detection process using a CNN. This experiment demonstrates the measurement of the peak wavelengths of complex overlapping FBGs resulting from the multiplexing of FBGs of the same wavelength to improve the performance of wavelength-division multiplexing.

B. Design Flow of Peak Detection With CNN

CNN training is important to accurately detect overlapping FBGs. Therefore, the peak detection process using CNN was developed according to the design flow shown in Fig. 2. Training data of tens of thousands of samples are required to improve the accuracy of the CNN. Training data should include the spectral patterns of overlapping FBGs under various conditions. It is not practical to collect a large amount of experimental training data. Therefore, it is necessary to create a numerical model of the FBG to generate the training data. The design process first used an optical spectrum analyzer to acquire the spectrum of each FBG (see Section II-C). The design process then performed a Gaussian approximation of the collected spectra to create a numerical model for each FBG. By adding the numerical models of each FBG that varied under various conditions, training data simulating overlapping could be created in a short time. Here, noise was added to the created training data to improve the performance of peak detection with CNN [30], [31]. The added noise used for noise-additive learning was provided as random numbers in a normal distribution. The effectiveness of the noise addition is discussed in Section III-A. These training data were used to train the CNN and develop a high-performance peak-detection process. The training was performed using a processor with an Intel Core i7-9800X CPU, NVIDIA GeForce RTX 3070 TI, and 32 GB RAM. In addition, MATLAB (MathWorks) was used as the software environment. The Deep Learning Toolbox in MATLAB was used for designing, training, and analyzing deep learning networks. The Parallel Computing Toolbox was also deployed to reduce the training time for deep learning in GPU processing.

C. Creation of Numerical Models of FBG and Training Data

First, the reflectance spectrum of each FBG was measured using an optical spectrum analyzer to create a numerical model for each FBG [see Fig. 3(I)]. Fig. 3(I-a)–(I-c) shows the results for FBG_{11} ($\Delta\lambda_{B\_11}$ – 0.2 nm), FBG_{12} ($\Delta\lambda_{B\_12}$ – 0.4 nm), and FBG_{13} ($\Delta\lambda_{B\_13}$ – 0.7 nm), respectively, at a Bragg wavelength of 1550 nm. Here, the spectrum of each FBG as shown in Fig. 3(I-a)–(I-c) can be observed by alternatively connecting the three branched couplers as the experimental setup shown in Fig. 1(a). The reflectance spectra of each FBG with different FWHMs were observed. Fig. 3(I-d) shows the results for all FBGs being connected, overlapped, and observed simultaneously. Using the results in Fig. 3(I-a)– (I-c), a numerical model was generated using the Gaussian approximation of the following equation [24]:

$$R_{ij}\left(\lambda, \lambda_{B\_ij}\right) = I_{\text{peak}\_ij} \exp\left[-4\ln 2\left(\frac{\lambda - \lambda_{B\_ij}}{\Delta\lambda_{B\_ij}}\right)^2\right] \quad (1)$$

where $i = 1, 2$ and $j = 1, 2, 3$.

Here, I_{peak_ij} is the intensity of the FBG, λ_{B_ij} is the Bragg wavelength of the FBG, and $\Delta\lambda_{B\_ij}$ is the FWHM of the FBG. i is the address in the wavelength multiplexing direction of the FBG. j is the address in the FWHM multiplexing direction of the FBG.

Fig. 3(II-a)–(II-c) shows the results of the numerical modeling of each FBG. Each numerical model agrees well with the spectrum of each FBG obtained in the experiment. Fig. 3(II-d) shows the results of adding the numerical models for each FBG. The spectra are generally consistent with the overlapped

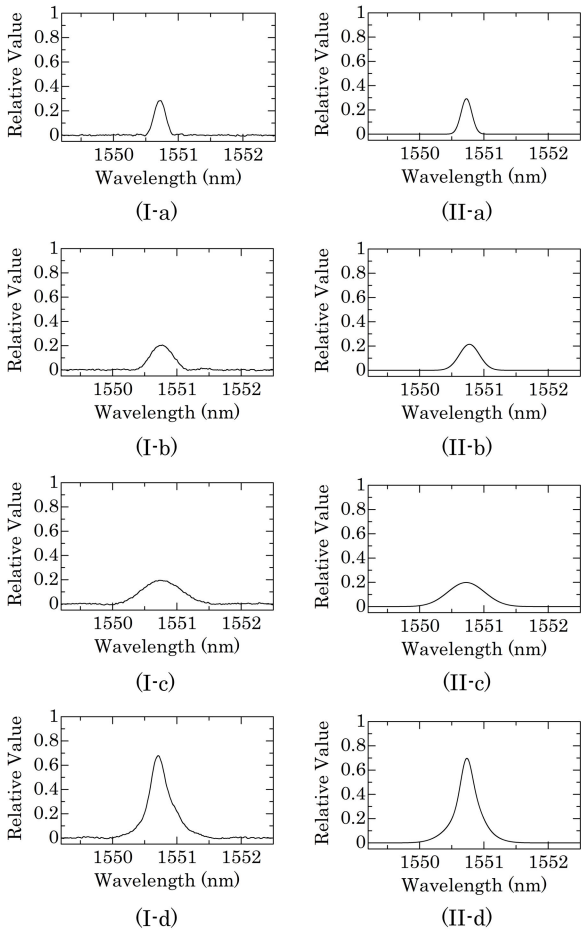

Fig. 3. Numerical modeling using Gaussian approximation. (I) Experimental results. (II) Numerical models. (a) FBG_{11}. (b) FBG_{12}. (c) FBG_{13}. (d) Multiplexed FBGs.

FBG spectra as shown in Fig. 3(I-d). Therefore, numerical models of each FBG were added by changing the Bragg wavelengths under various conditions to produce the training data. The training data were targeted for FBG_{11}, FBG_{12}, and FBG_{13} (1550 nm) with a wavelength range of 1549.2–1552.5 nm, wavelength resolution of 2 pm, 1651 data points, and 150 579 data sets. Similarly, numerical models were created for FBG_{21}, FBG_{22}, and FBG_{23} (1555 nm), with a wavelength range of 1554.2–1557.5 nm, a wavelength resolution of 2 pm, 1651 data points, and 150 579 data sets. In addition, noise was added to the training data to improve the performance of peak detection with the CNN. The amplitude of the noise addition was set to 5% of that of the FBG signals.

D. Design and Training of Peak Detection With CNN

The experiments were conducted in a configuration where the peak detection modules corresponding to the peak wavelength of each FBG were arranged in parallel, as shown in Fig. 4. This figure shows the measurement design of the three FBGs in the 1550 nm wavelength range. First, the spectra of the overlapped FBGs in the wavelength range of 1549.2–1552.5 nm were acquired with an optical spectrum

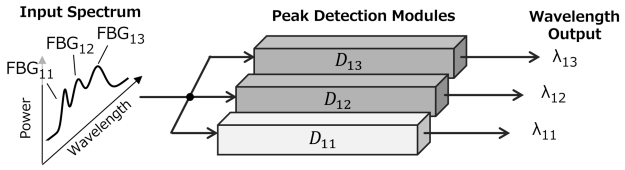

Fig. 4. Concept of FBG measurement with peak detection modules.

analyzer. The acquired spectra were input into the parallelized modules D_{11}, D_{12}, and D_{13}. Each module was optimized to detect the peak wavelengths corresponding to FBG_{11}, FBG_{12} and FBG_{13}. Each module outputs the peak wavelength corresponding to each FBG.

The design of the peak detection module D_{11} for FBG_{11} with a CNN is shown in Fig. 5. The CNN was designed based on convolutional layers [32], [33]. The CNN operates by optimizing the filters and weights in each layer through iterative learning using the training data. The module with the CNN was designed with four convolutional layers. First, the FBG spectrum was passed through the input layer. The input data were then fed into the convolution layer. In the convolution layer, the features were extracted by a convolution filter with 64 filters and a kernel size of 21 $\times$ 1. Therefore, the feature data were expanded to 64 types compared with the input data. The extracted feature data were adjusted to equalize the data size with the input data by the padding process. To make the feature extraction more active, the output was generated using ReLU. ReLU, also called a ramp function, is a simple activation function and is known to have characteristics that allow for fast computational processing. For this reason, it is widely used as an activation function in the field of deep learning. The output feature data were downsampled using a pooling layer to prevent the number of features from becoming too large and to aggregate them. The pool size used to determine the compression ratio was 2 $\times$ 1. The iterations of the convolution and pooling layers aggregated the feature data that were important for FBG_{11} peak detection. The aggregated feature data were input into the flat layer. The flat layer converts the 2-D feature data into 1-D format. Finally, the module uses the dense layer to multiply and aggregate the feature data by weights and convert them to the desired peak wavelength λ_{B_11} for FBG_{11}. In this study, the dense layer multiplies the 13 814 $\times$ 1 feature matrix by a 1 $\times$ 13 814 weight matrix, and a bias is added to the results to obtain the desired wavelength data (a 1 $\times$ 1 matrix). The optimization algorithm for learning used Adam. Adam is similar to a method called root mean squared propagation (RMSProp), but it uses parameter updates with an additional momentum term. This is a typical optimization algorithm in deep learning. Modules for peak detection have been developed for FBG_{12} and FBG_{13}. Furthermore, for FBG_{21}, FBG_{22}, and FBG_{23} with different wavelength regions, modules corresponding to the wavelength range of 1554.2–1557.5 nm were developed simultaneously.

Fig. 6 shows the results of training four-layer CNN. Training performance was evaluated using the root-mean-square

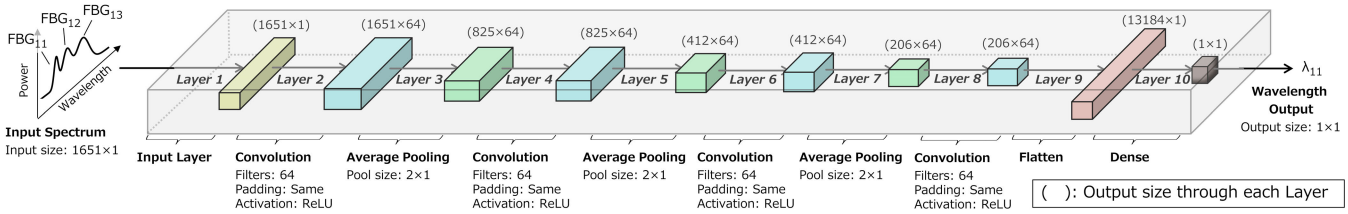

Fig. 5. Design of peak detection module D_{11} with CNN for FBG_{11}.

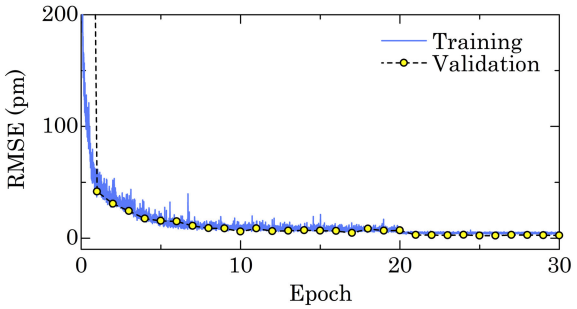

Fig. 6. Variation of RMSE with number of epochs.

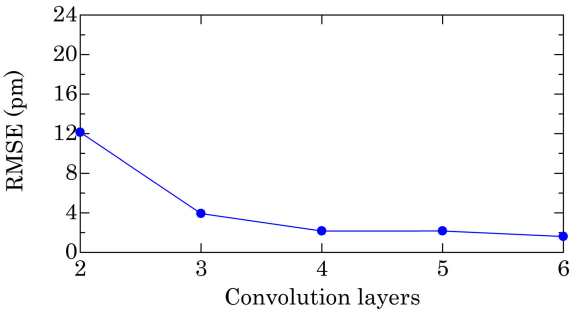

Fig. 7. Variation of RMSE with number of convolution layers.

error (RMSE) defined by the following equation [24]:

$$\mathrm{RMSE} = \sqrt{\frac{\sum_{i=1}^{n}\sum_{j=1}^{m}\left(\lambda_{B\_ij} - \lambda_{ij}\right)^2}{n \times m}} \tag{2}$$

where $n = 2$ and $m = 3$.

Here, λ_{ij} is the Bragg wavelength predicted by the CNN. n is the number of FBGs in the wavelength multiplexing direction. m is the number of FBGs in the FWHM multiplexing direction.

An epoch is an indicator of the number of training sessions, and one epoch represents the progression of training using 150579 training data sets. Using the same numerical model as the training data, 150579 validation data sets were created. As a result of the training, a peak-detection performance of approximately 2 pm was achieved at epoch 30 in the validation data.

Next, to examine in detail the peak detection performance using CNN, the RMSE for different numbers of convolution layers was calculated. The number of epochs was set as 30. Fig. 7 shows the RMSE results with respect to the number of convolution layers. The RMSE is significantly improved beyond the three layers, indicating that sufficient features have been extracted and aggregated. The RMSE for the four-layer CNN was accurate to approximately 2 pm. The trained module attempted the peak detection process 10 000 times, requiring a peak detection time of approximately 3 ms/attempt. Therefore, subsequent experiments used the four-layer CNN to detect the peak of each FBG.

III. Experimental Results

A. FBG Strain Measurements With CNN and Noise Addition

First, the strain measurements of FBG_{11}, FBG_{12}, and FBG_{13} (1550 nm) were evaluated using the peak detection process with CNN. In addition, to verify the effectiveness of noise-additive learning, the study compared learning without and with 5% noise added to the signal amplitude of the FBG. Fig. 8(I) shows the results of the numerical simulations using the numerical model and Fig. 8(II) shows the results of the experiments. Fig. 8(I-a) and (II-a) shows the strain conditions applied to each FBG; the numerical simulations and experimental conditions were identical. The applied range of strain was 0–1000 $\mu\varepsilon$, and the step size was 50 $\mu\varepsilon$. The strain was applied via tension using a movable stage installed in each FBG. The experiment was conducted under different conditions of strain application, and 43 measurements were obtained. Fig. 8(I-b) and (II-b) shows the results of the FBG spectra in the numerical simulations and experiments, respectively. FBGs with different FWHMs produce complex overlapping states owing to wavelength changes caused by the strain. The experiments showed that the spectra were in good agreement with the numerical simulations. Because of this complex spectral variation in overlapped FBGs, it is difficult to detect the peak wavelengths of individual FBGs with high precision using conventional peak detection processing.

Fig. 8(I-c) and (II-c) shows the results of the peak wavelength detection with the CNN trained without noise. The numerical simulation in Fig. 8(I-c) detects the change in the peak wavelength of each FBG with respect to the strain from a complex overlapping spectrum. This suggests that the CNN is useful as a peak detection process for overlapping FBGs. On the other hand, the experiment in Fig. 8(II-c) shows that, although the peak wavelengths of each FBG can be tracked, the detection performance is much worse than that in the numerical simulation. This is likely due to the fact that the FBG spectrum of the experiment, including the effects of noise and other factors, does not perfectly match the ideal Gaussian distribution curve, as evidenced by the results in Fig. 3, and the accuracy is reduced by the gap with the numerical model.

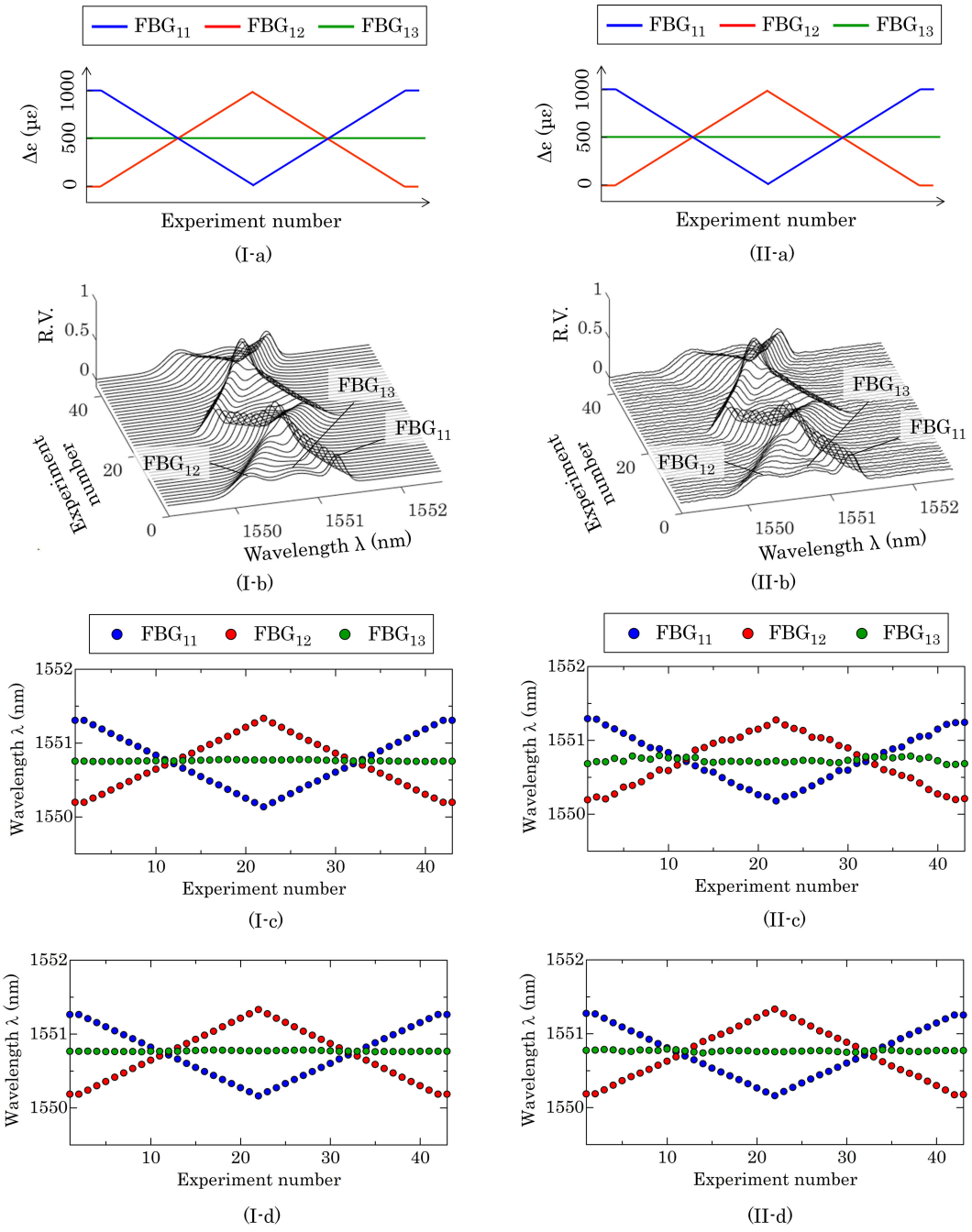

Fig. 8. Strain measurements of multiplexed FBGs with the same wavelength. (I) Simulation results. (II) Experimental results. (a) Strain condition. (b) Spectra of three FBGs. (c) Peak wavelengths using CNN trained with 0% noise. (d) Peak wavelengths using CNN trained with 5% noise.

To increase the tolerance to such variations in the experimental signal, noise-additive learning was introduced.

Fig. 8(I-d) and (II-d) shows the results of the CNN trained with 5% noise-additive learning. In spite of the complex overlapping of the three FBGs, a change in the peak wavelength of each FBG with strain was clearly observed in the experiment. It is clear that the introduction of noise-additive learning can significantly improve the performance of the peak wavelength detection. The maximum change in peak wavelength with respect to strain is 1.10 nm for FBG_{11} and 1.15 nm for FBG_{12} in the numerical simulations. In the experiment, the values for FBG_{11} and FBG_{12} are 1.11 and 1.15 nm, respectively, which indicates that their values are in good agreement. This indicates that CNN with noise-additive learning is effective in improving the performance of wavelength-division multiplexing because it is flexible enough to handle complex overlapping where the wavelength of the multiple FBGs changes independently. It was also demonstrated that the three FBGs could be detected in spite of the complex overlapping between them.

The relationship between the peak wavelength and strain was analyzed to further evaluate the peak detection

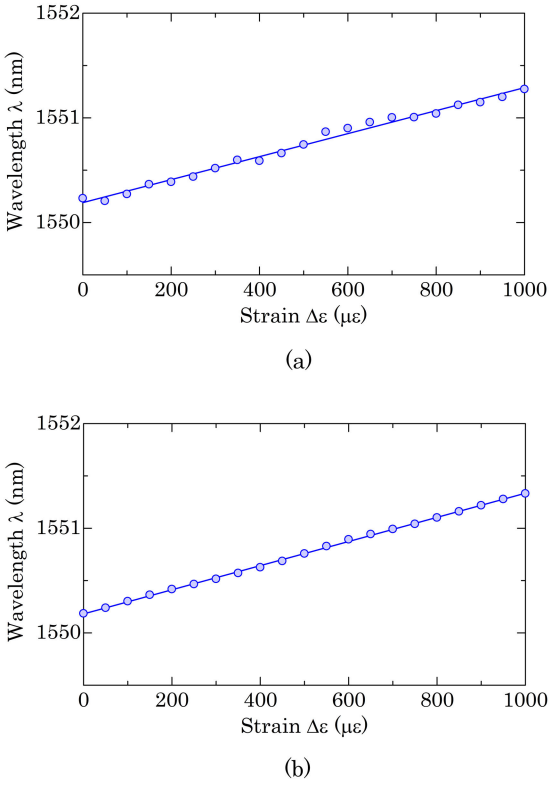

Fig. 9. Response of peak wavelength to strain in FBG_{12}. (a) CNN trained with 0% noise. (b) CNN trained with 5% noise.

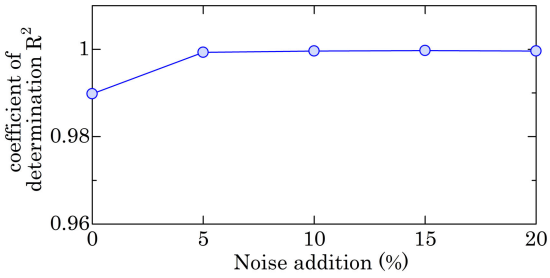

Fig. 10. Evaluation of coefficient of determination by CNN trained with noise addition for FBG_{12}.

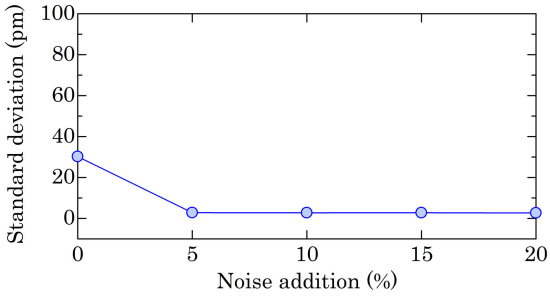

Fig. 11. Evaluation of standard deviation by CNN trained with noise addition.

performance in detail. Fig. 9(a) and (b) shows the results of analyzing the peak wavelengths due to the strain on FBG_{12} for CNN trained with 0% and 5% noise in Fig. 8(II-c) and (II-d), respectively. In the case of noise addition, the linearity of the wavelength with respect to the strain improved. The sensitivity of the peak wavelength to strain when noise was applied was approximately 1.15×10^{-3} nm/$\mu\varepsilon$. This is in good agreement with the commonly known sensitivity of FBGs.

Next, the effect of the noise magnitude applied in the CNN training on peak detection performance was examined. The effect of noise on the linearity of the peak detection performance was first evaluated. The coefficient of determination (R^2), which represents the linearity of the wavelength response to the strain in Fig. 9, was calculated. Noise-additive learning was applied in the range of 0%–20% of the FBG signal intensity. Fig. 10 shows the R^2 results for the CNN trained with added noise. The value with noise at 0% was 0.9898, whereas the value with noise at 5% improved to 0.9993 and then remained almost unchanged.

To further evaluate the wavelength resolution of the CNN, experiments were validated with a constant strain on each FBG, and the standard deviation of the peak wavelength of each FBG was calculated. Fig. 11 shows the results of the mean of the standard deviations of all FBGs for the CNN trained with added noise. The value with noise at 0% is 30.2 pm, while the value with noise at 5% is significantly improved to 2.8 pm. Later, the value with noise remained almost unchanged. This indicates that the introduction of noise-additive learning can significantly improve the performance of the FBG peak detection. In subsequent experiments, peak wavelengths were calculated using CNN trained with 5% noise.

Furthermore, the presence and absence of a Gaussian filter in the smoothing preprocessing of the experimental data were evaluated. It was determined that the standard deviation to noise was constant with and without the Gaussian filter. Therefore, it was found that noise-additive learning can reduce the standard deviation even when a Gaussian filter is not used as a preprocessing step. However, in this experiment, the Gaussian filter was introduced to reduce noise and to create a numerical model of the Gaussian approximation as shown in Fig. 3.

To verify the performance of noise-additive learning in detail, RMSE was calculated from the experimental values. The reference wavelengths for calculating RMSE were obtained by peak detection from the spectrum of each FBG in Fig. 3(I-a) –(I-c), respectively. The measurement wavelengths were calculated using CNN by observing the overlapped FBGs. The RMSE was 127 and 11 pm with the noise at 0% and 5%, respectively. When the noise was further increased, the RMSE values remained unchanged. Noise-additive learning was found to be effective in improving both the standard deviation and RMSE of peak wavelength detection.

B. Verification of Combining Same Wavelength Multiplexing and Different-Wavelength Multiplexing

Next, to evaluate the effectiveness of peak detection with CNN for combining same-wavelength and different-wavelength multiplexing, simultaneous measurements of multiplexed FBGs in the 1550 and 1555 nm wavelength regions were performed. The spectra in each wavelength region were

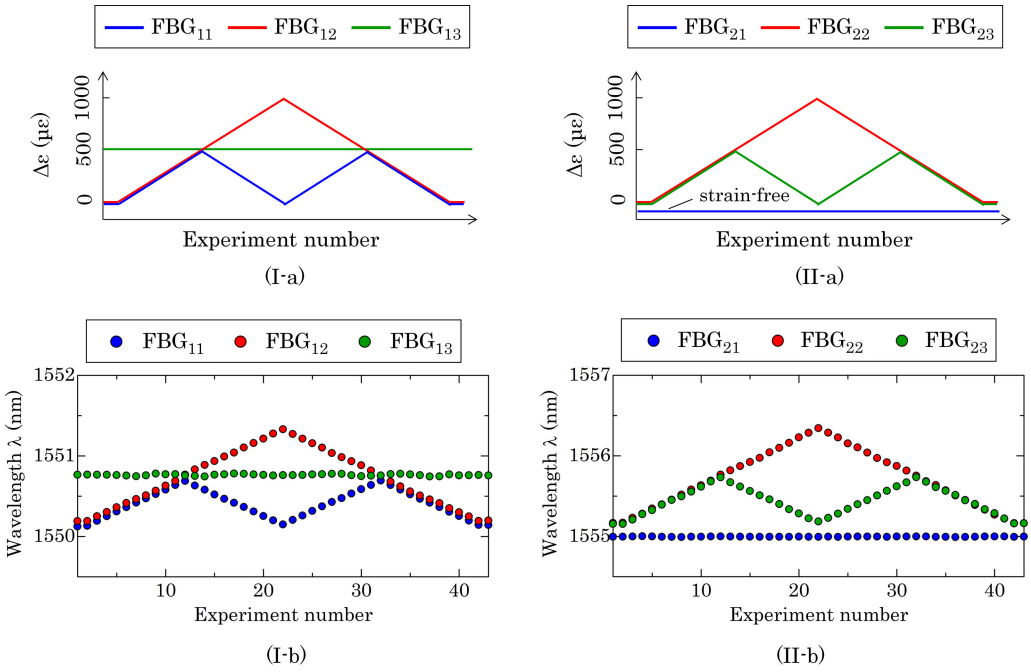

Fig. 12. FBG measurements combining same- and different-wavelength multiplexing. (I) FBG_{11}, FBG_{12}, and FBG_{13} with 1550 nm. (II) FBG_{21}, FBG_{22}, and FBG_{23} with 1555 nm. (a) Strain condition. (b) Peak wavelengths using CNN.

analyzed using each peak detection module with a CNN corresponding to each FBG, as shown in Fig. 4. Fig. 12(I) shows the results for FBG_{11}, FBG_{12}, and FBG_{13} (1550 nm) and Fig. 12(II) for FBG_{21}, FBG_{22}, and FBG_{23} (1555 nm). Fig. 12(I-a) and (II-a) shows the strain conditions of the FBGs in each wavelength range. FBG_{21} was strain free. Fig. 12(I-b) and (II-b) shows the peak wavelength results, where the wavelength variation with strain was clearly observed for each FBG in each wavelength range. The peak wavelength changes with the strain levels of up to 500 $\mu\varepsilon$ for FBG_{11} and FBG_{23} and 1000 $\mu\varepsilon$ for FBG_{12} and FBG_{22}. The changes in peak wavelength were 0.56 and 0.58 nm for FBG_{11} and FBG_{23}, respectively, and 1.14 and 1.17 nm for FBG_{12} and FBG_{22}, respectively. The strain condition in Fig. 12 has a long section where the strain levels of FBG_{11}, FBG_{12}, FBG_{22}, and FBG_{23} were identical and completely overlapped, but the peak wavelengths of each FBG were detected without interference. The wavelength sensitivity to strain was approximately 1.11×10^{-3} nm/$\mu\varepsilon$ ($R^2 = 0.9997$) for FBG_{11}, 1.15×10^{-3} nm/$\mu\varepsilon$ ($R^2 = 0.9993$) for FBG_{12}, 1.17×10^{-3} nm/$\mu\varepsilon$ ($R^2 = 0.9997$) for FBG_{22}, and 1.16×10^{-3} nm/$\mu\varepsilon$ ($R^2 = 0.9993$) for FBG_{23}. In this experiment, it was found that the developed peak detection method is effective for multipoint and simultaneous measurement of FBGs for same-wavelength multiplexing and different-wavelength multiplexing.

FBG measurements with a small strain were performed to evaluate the wavelength resolution for peak detection. Fig. 13(a) shows the strain conditions. Each FBG was subjected to a small strain in the range of 0–100 $\mu\varepsilon$ in 5 $\mu\varepsilon$ steps. Fig. 13(b) shows the peak wavelength results for each FBG, where the peak wavelength was detected in response to a small strain. FBG_{22} responded with a wavelength shift of 0.13 nm for a strain of 100 $\mu\varepsilon$, and FBG_{23} responded with

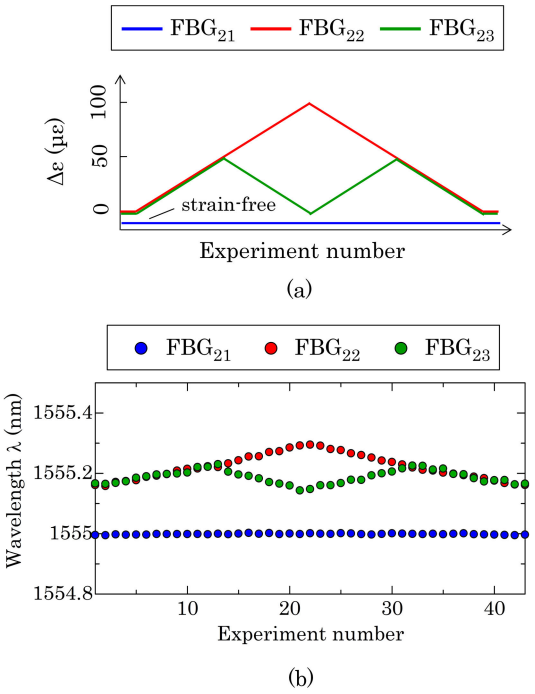

Fig. 13. Consideration for small strain measurement. (a) Strain condition. (b) Peak wavelengths.

a wavelength shift of 0.06 nm for a strain of 50 $\mu\varepsilon$. The standard deviation of the wavelength from the peak detection of the experimental results as shown in Fig. 11 is 2.8 pm, which corresponds to a strain resolution of approximately 2.5 $\mu\varepsilon$. The results of the above-mentioned experiments show that the peak detection process using the CNN can analyze three overlapped FBGs over a wide strain range, and it was

experimentally demonstrated that it can improve the performance of wavelength-division multiplexing.

IV. Discussion

Most AI model studies on overlap limit the wavelengths of a large number of overlapping FBGs to fixed values. Therefore, many studies have focused on the problem of simple overlaps where only one FBG changes with wavelength. However, it is difficult for the models developed in this way to accommodate arbitrary wavelength changes of individual FBGs. In actual industrial applications, it is essential that each installed sensor operates independently. However, the AI model research has yet to demonstrate a model that can accurately analyze arbitrary wavelength changes of even two overlapped FBGs, and solving this problem is an important challenge. This article is the first to address the problem of arbitrary wavelengths with three overlapping FBGs using an AI model. In this report, the wavelengths of FBGs are arbitrarily varied, so it is necessary to construct a data set that includes more complex overlap conditions than that in previous studies. Therefore, the model for arbitrary wavelengths was slightly less accurate than the model focusing on a single FBG. However, we found that introducing noise-additive learning improved the standard deviation and RMSE by almost an order of magnitude. The developed model is the first to solve the problem of overlapping three FBGs for arbitrary wavelength changes. Furthermore, it is clear that the AI model is effective for measuring FBGs in different wavelength regions.

In actual FBGs, small variations in the FWHM may occur due to manufacturing. Therefore, we attempted to evaluate the AI model for small variations in the FWHM. FBG_{12} with an FWHM of approximately 0.4 nm was used for the evaluation. The evaluation was done by increasing or decreasing the FWHM of the numerical model by up to 5% from the original value. The experiment used 5% noise-additive learning, as shown in Fig. 9, to evaluate the linearity of FBG_{12} for different FWHMs of the numerical model. As a result, the slope and coefficient of determination were almost the same for variations within 5%. This indicates that the developed AI model may be able to tolerate small variations in the FWHM.

To advance the use of AI models in practical industrial applications, it is important to increase the number of FBG sensors that can operate with arbitrary wavelengths. This requires a large number of data sets to accommodate the more complex overlaps resulting from an increase in the number of sensors. The current number of data sets is based on the upper limit that the model can handle without encountering memory overflow in the Windows OS environment. Therefore, the number of data sets can be improved through memory augmentation to enhance the AI model.

V. Conclusion

In this study, we proposed an FBG peak detection method using a CNN to improve the wavelength-division multiplexing performance. The CNN was designed using four convolutional layers. Training was performed using a numerical model of the FBG with the Gaussian approximation. The developed CNN showed high accuracy for numerical simulations but significantly lower accuracy in experiments. To address this problem, we introduced noise-additive learning to increase tolerance to variations in the experimental signal. This significantly improved the standard deviation of peak wavelength detection from 30.2 to 2.8 pm in the experiment. Consequently, an experimental demonstration of the peak wavelength measurement of three complex overlapping FBGs was successfully achieved. Furthermore, it was demonstrated that the method could be applied to same-wavelength multiplexing and different-wavelength multiplexing, and that it could be applied to a wide range of strains. The method using a CNN does not require special optical adjustments and can improve the wavelength division multiplexing performance through computational processing at a low cost. The experimental demonstration using three overlapped FBGs contributes to the ability to triple the performance of wavelength-division multiplexing.

In this study, it was shown that the peak wavelengths of three FBGs can be measured with a simple network design and that noise-additive learning can improve peak detection performance. AI models are known to be powerful tools that use data representative of the problem domain to extract the desired features. However, due to the vast number of tunable parameters and the high freedom in layer design, it can take a substantial amount of time to optimize the AI model to a practical stage, particularly for a complex AI model like the present one that handles arbitrary wavelengths of FBGs. In this article, as the first AI model designed to handle arbitrary wavelengths of FBGs, we chose CNN, which are widely used in various fields and are a standard technique in deep learning. Our future work aims to find a more optimal AI model for arbitrary wavelengths. The advantages of using CNN for peak detection are its high learning performance, picometer resolution, millisecond-order computation time, and ability to handle complex overlaps due to arbitrary changes in wavelength. In the future, we plan to use deep learning to verify the design of networks that can multiplex more FBGs of the same wavelength.

References

[1] J. M. Lopez-Higuera, *Handbook of Optical Fibre Sensing Technology*. Hoboken, NJ, USA: Wiley, 2001.

[2] E. J. Friebele et al., "Optical fiber sensors for spacecraft applications," *Smart Mater. Struct.*, vol. 8, no. 6, pp. 813–838, Dec. 1999.

[3] Y. Mizuno, N. Hayashi, H. Fukuda, K. Y. Song, and K. Nakamura, "Ultrahigh-speed distributed Brillouin reflectometry," *Light, Sci. Appl.*, vol. 5, no. 12, Jun. 2016, Art. no. e16184.

[4] D. Huang, Y. Shi, F. Li, and P. K. A. Wai, "Fourier domain mode locked laser and its applications," *Sensors*, vol. 22, no. 9, p. 3145, Apr. 2022.

[5] V. S. Chaudhary, D. Kumar, B. P. Pandey, and S. Kumar, "Advances in photonic crystal fiber-based sensor for detection of physical and biochemical parameters—A review," *IEEE Sensors J.*, vol. 23, no. 2, pp. 1012–1023, Jan. 2023.

[6] V. S. Chaudhary, D. Kumar, and S. Kumar, "Au-TiO_2 coated photonic crystal fiber based SPR refractometric sensor for detection of cancerous cells," *IEEE Trans. Nanobiosci.*, early access, Nov. 3, 2022, doi: 10.1109/TNB.2022.3219104.

[7] A. Kersey et al., "Fiber grating sensors," *J. Lightw. Technol.*, vol. 15, no. 8, pp. 1442–1463, Aug. 1997.

[8] A. Othonos and K. Kalli, *Fiber Bragg Gratings*. Norwood, MA, USA: Artech House, 1999.

[9] Q. Rong et al., "Ultrasonic imaging of seismic physical models using fiber Bragg grating Fabry–Pérot probe," *IEEE J. Sel. Top. Quantum Electron.*, vol. 23, no. 2, Mar./Apr. 2017, Art. no. 5600506.

[10] T. Yamaguchi, K. Ishihara, and Y. Shinoda, "Field-programmable gate array-based multichannel measurement system for interrogating fiber Bragg grating sensors," *IEEE Sensors J.*, vol. 19, no. 15, pp. 6163–6172, Aug. 2019.

[11] T. Yamaguchi, W. Endo, and Y. Shinoda, "High-speed interrogation system for fiber Bragg gratings with buffered Fourier domain mode-locked laser," *IEEE Sensors J.*, vol. 21, no. 15, pp. 16659–16669, Aug. 2021.

[12] N. Sonoda, R. Takagi, I. Saito, T. Abe, S. Zhao, and Y. Tanaka, "Multipoint bending measurement using multicore fiber Bragg grating and two-photon absorption process in Si-APD," *IEEE Sensors J.*, vol. 21, no. 22, pp. 25736–25742, Nov. 2021.

[13] Y. Yu, L. Lui, H. Tam, and W. Chung, "Fiber-laser-based wavelength-division multiplexed fiber Bragg grating sensor system," *IEEE Photon. Technol. Lett.*, vol. 13, no. 7, pp. 702–704, Jul. 2001.

[14] Z. Luo, H. Wen, H. Guo, and M. Yang, "A time- and wavelength-division multiplexing sensor network with ultra-weak fiber Bragg gratings," *Opt. Exp.*, vol. 21, no. 19, pp. 22799–22807, Sep. 2013.

[15] K. Yuksel, V. Moeyaert, P. Mégret, and M. Wuilpart, "Complete analysis of multireflection and spectral-shadowing crosstalks in a quasi-distributed fiber sensor interrogated by OFDR," *IEEE Sensors J.*, vol. 12, no. 5, pp. 988–995, May 2012.

[16] M. Zhu and H. Murayama, "Fast demodulation of OFDR based long length FBG sensing system for noisy signals," *Opt. Exp.*, vol. 26, no. 16, pp. 19804–19814, Aug. 2018.

[17] T. Yamaguchi, M. Arai, and Y. Shinoda, "Development of wavelength measurement system of multiplex fiber Bragg gratings using optical frequency domain reflectometry," in *Proc. ICST*, Auckland, New Zealand, Dec. 2015, pp. 425–429.

[18] C. Z. Shi, C. C. Chan, W. Jin, Y. B. Liao, Y. Zhou, and M. S. Demokan, "Improving the performance of a FBG sensor network using a genetic algorithm," *Sens. Actuators A, Phys.*, vol. 107, no. 1, pp. 57–61, Oct. 2003.

[19] J. J. Liang, P. N. Suganthan, C. C. Chan, and V. L. Huang, "Wavelength detection in FBG sensor network using tree search DMS-PSO," *IEEE Photon. Technol. Lett.*, vol. 18, no. 12, pp. 1305–1307, Jun. 26, 2006.

[20] J. Chen, H. Jiang, T. Liu, and X. Fu, "Wavelength detection in FBG sensor networks using least squares support vector regression," *J. Opt.*, vol. 16, no. 4, Mar. 2014, Art. no. 045402.

[21] H. Jiang, J. Chen, and T. Liu, "Wavelength detection in spectrally overlapped FBG sensor network using extreme learning machine," *IEEE Photon. Technol. Lett.*, vol. 26, no. 20, pp. 2031–2034, Oct. 15, 2014.

[22] H. Jiang et al., "Wavelength detection of model-sharing fiber Bragg grating sensor networks using long short-term memory neural network," *Opt. Exp.*, vol. 27, no. 15, pp. 20583–20596, Jul. 2019.

[23] Y. C. Manie et al., "Enhancement of the multiplexing capacity and measurement accuracy of FBG sensor system using IWDM technique and deep learning algorithm," *J. Lightw. Technol.*, vol. 38, no. 6, pp. 1589–1603, Mar. 15, 2020.

[24] B. Li, Z. W. Tan, P. P. Shum, C. Wang, Y. Zheng, and L. J. Wong, "Dilated convolutional neural networks for fiber Bragg grating signal demodulation," *Opt. Exp.*, vol. 29, no. 5, pp. 7110–7123, Feb. 2021.

[25] A. Venketeswaran et al., "Recent advances in machine learning for fiber optic sensor applications," *Adv. Intell. Syst.*, vol. 4, no. 1, Jan. 2022, Art. no. 2100067.

[26] O. Furukawa, "A study on thermal detection based on support vector machine using dynamic time warping and application to optical fiber sensor," *IEEE Sensors J.*, vol. 21, no. 5, pp. 6325–6334, Mar. 2021.

[27] J. N. Caceres, K. Noda, G. Zhu, H. Lee, K. Nakamura, and Y. Mizuno, "Spatial resolution enhancement of Brillouin optical correlation-domain reflectometry using convolutional neural network: Proof of concept," *IEEE Access*, vol. 9, pp. 124701–124710, 2021.

[28] J. Pons, O. Slizovskaia, R. Gong, E. Gomez, and X. Serra, "Timbre analysis of music audio signals with convolutional neural networks," in *Proc. USIPCO*, Kos, Greece, Aug. 2017, pp. 2744–2748.

[29] D. R. Sarvamangala and R. V. Kulkarni, "Convolutional neural networks in medical image understanding: A survey," *Evol. Intell.*, vol. 15, no. 1, pp. 1–22, Jan. 2021.

[30] T. Ko, V. Peddinti, D. Povey, M. L. Seltzer, and S. Khudanpur, "A study on data augmentation of reverberant speech for robust speech recognition," in *Proc. ICASSP*, New Orleans, LA, USA, Mar. 2017, pp. 5220–5224.

[31] Y. Li, H. Wang, L. M. Dang, A. Sadeghi-Niaraki, and H. Moon, "Crop pest recognition in natural scenes using convolutional neural networks," *Comput. Electron. Agricult.*, vol. 169, Feb. 2020, Art. no. 105174.

[32] C.-C.-J. Kuo, "The CNN as a guided multilayer RECOS transform [lecture notes]," *IEEE Signal Process. Mag.*, vol. 34, no. 3, pp. 81–89, May 2017.

[33] R. C. Gonzalez, "Deep convolutional neural networks," *IEEE Signal Process. Mag.*, vol. 35, no. 6, pp. 79–87, Nov. 2018.

Tatsuya Yamaguchi (Member, IEEE) received the B.S., M.S., and Ph.D. degrees in engineering from Nihon University, Tokyo, Japan, in 2013, 2015, and 2018, respectively.

He then joined the Department of Electrical Engineering, Nihon University. His current research interests include optical measurements, digital signal processing, structural health monitoring, and optical fiber sensing.

Dr. Yamaguchi is a member of the Institute of Electrical Engineers of Japan (IEEJ) and the Society of Instrument and Control Engineers (SICE).

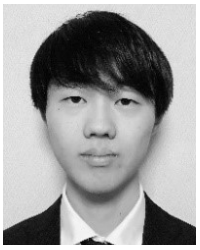

Hiroto Kawashima received the B.S. degree in engineering from Nihon University, Tokyo, Japan, in 2022, where he is pursuing the M.S. degree.

His current research interests include optical fiber sensing.

Mr. Kawashima is a Student Member of the Institute of Electrical Engineers of Japan (IEEJ).

Hiroki Matsuda received the B.S. degree in engineering from Nihon University, Tokyo, Japan, in 2022, where he is pursuing the M.S. degree.

His current research interests include optical fiber sensing.

Mr. Matsuda is a Student Member of the Institute of Electrical Engineers of Japan (IEEJ).

Yukitaka Shinoda (Member, IEEE) received the B.Sc., M.Sc., and Ph.D. degrees in electrical engineering from Nihon University, Tokyo, Japan, in 1987, 1989, and 2004, respectively.

He was a Visiting Researcher with the Virginia Polytechnic Institute and State University (Virginia Tech), Blacksburg, VA, USA, from 2009 to 2010. Since 2012, he has been a Professor with the College of Science and Technology, Nihon University. He has focused on laser sensing, digital signal processing, motion analysis, and optical scanning holography.

Dr. Shinoda is a member of the Institute of Electrical Engineers of Japan (IEEJ), the Society of Instrument and Control Engineers (SICE), and the Japan Society of Applied Physics (JSAP).